ADVANCED FUNCTIONAL MATERIALS
www.afm-journal.de

Materials Views
www.MaterialsViews.com

Photophysics of Molecular-Weight-Induced Losses in Indacenodithienothiophene-Based Solar Cells

Nicola Gasparini, Athanasios Katsouras, Mamantos I. Prodromidis, Apostolos Avgeropoulos, Derya Baran, Michael Salvador, Stefanie Fladischer, Erdmann Spiecker, Christos L. Chochos, Tayebeh Ameri,* and Christoph J. Brabec*

The photovoltaic performance and optoelectronic properties of a donor–acceptor copolymer are reported based on indacenodithienothiophene (IDTT) and 2,3-bis(3-(octyloxy)phenyl)quinoxaline moieties (PIDTTQ) as a function of the number-average molecular weight (M_n). Current–voltage measurements and photoinduced charge carrier extraction by linear increasing voltage (photo-CELIV) reveal improved charge generation and charge transport properties in these high band gap systems with increasing M_n, while polymers with low molecular weight suffer from diminished charge carrier extraction because of low mobility–lifetime ($\mu\tau$) product. By combining Fourier-transform photocurrent spectroscopy (FTPS) with electroluminscence spectroscopy, it is demonstrate that increasing M_n reduces the nonradiative recombination losses. Solar cells based on PIDTTQ with $M_n = 58$ kD feature a power conversion efficiency of 6.0% and a charge carrier mobility of 2.1×10^{-4} cm^2 V^{-1} s^{-1} when doctor bladed in air, without the need for thermal treatment. This study exhibits the strong correlations between polymer fractionation and its optoelectronics characteristics, which informs the polymer design rules toward highly efficient organic solar cells.

1. Introduction

High band gap (HBG) conjugated polymers ($E_g^{opt} \geq 1.7$ eV) with excellent photovoltaic properties, promising environmental stability, and up-scaling ability are highly desirable complementary absorbers for efficient organic tandem solar cells.[1] Contrary to the extensive efforts devoted to the development of low band gap (LBG) donor polymers, the investigation of HBG polymers with suitable photovoltaic properties in inverted architecture solar cells, particularly when processed in air using roll-to-roll compatible printing methods, is barely examined. Regioregular poly(3-hexyl thiophene) (rrP3HT) is the most widely employed high band gap polymer for tandem organic photovoltaics (OPVs) because of its reliable photovoltaic performance.[1] The rrP3HT-based solar cells with reasonable performances usually rely on time-consuming device fabrication processes such as thermal treatment and solvent vapor annealing, representing a limiting factor in high-throughput device manufacturing. Furthermore, the photovoltaic performance of most high efficiency HBG polymers is demonstrated in conventional device architectures, usually processed through spin coating in combination with solvent additives or with the help of thermal posttreatment.[2–9] OPVs based on regular device architecture typically suffer from oxidation of low work function metals and consequently low operating lifetimes.[10]

Donor–acceptor (D–A) conjugated polymers based on indacenodithiophene (IDT) or indacenodithieno[2,3] thiophene (IDTT) usually exhibit HBGs, depending on the choice of electron deficient unit. These polymers have demonstrated great promise as p-type polymers in OPVs.[7,11] IDT comprises two thiophene rings held in a rigid arrangement via a central phenyl ring (**Scheme 1**). It has emerged as a favorable electron rich building block because of its highly planar structure, which enables copolymers with improved charge carrier mobility. Additionally, good solubility is achieved because of the four alkyl side chains anchored on the periphery of the monomer.[11] Ting et al. synthesized random and alternating copolymers based on IDT and benzothiadiazole with an optical band gap $E_g^{opt} = 1.75$ eV. OPVs fabricated with this material resulted in

N. Gasparini, Dr. D. Baran, Dr. M. Salvador, Dr. S. Fladischer, Dr. T. Ameri, Prof. C. J. Brabec
Institute of Materials for Electronics and Energy Technology (I-MEET)
Friedrich-Alexander-University Erlangen-Nuremberg
Martensstraße 7, 91058 Erlangen, Germany
E-mail: nicola.gasparini@fau.de; tayebeh.ameri@fau.de

A. Katsouras, Dr. A. Avgeropoulos, Dr. C. L. Chochos
Department of Materials Science Engineering
University of Ioannina
Ioannina 45110, Greece

Dr. M. I. Prodromidis
Department of Chemistry
University of Ioannina
Ioannina 45110, Greece

Dr. M. Salvador
Instituto de Telecomunicações
Instituto Superior Técnico
Av. Rovisco Pais, P-1049-001 Lisboa, Portugal

Dr. S. Fladischer, Prof. E. Spiecker
Center for Nanoanalysis and Electron Microscopy (CENEM)
Friedrich-Alexander-University Erlangen-Nuremberg
Cauerstraße 6, 91058 Erlangen, Germany

Prof. C. J. Brabec
Bavarian Center for Applied Energy Research (ZAE Bayern)
Haberstrasse 2a, 91058 Erlangen, Germany

DOI: 10.1002/adfm.201501062

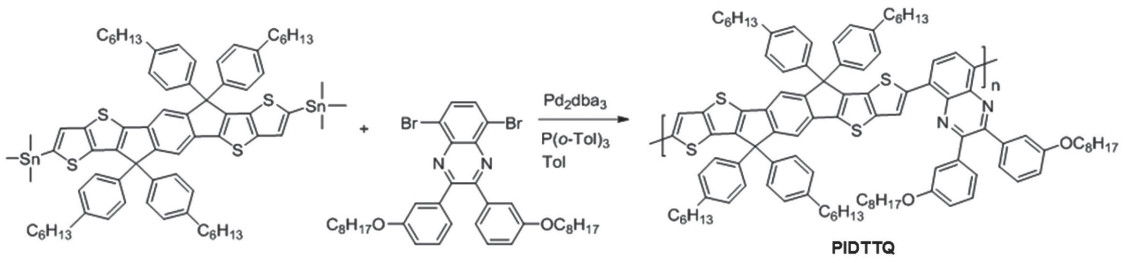

Scheme 1. Polymerization reaction towards the preparation of PIDTTQ.

maximum PCEs of 6.4%.[11] Jen et al. studied several high band gap IDT-based D–A copolymers with different electron deficient units.[7,11] The corresponding IDT-based copolymers presented deep HOMO levels, and hence led to relatively high open circuit voltages (V_{oc}) of 0.88 V and an overall PCE of 6.6%.[12] More recently, Wang et al. reported a PCE of 7.5% using an IDT–thiophene–quinoxaline–thiophene copolymer that carries *meta*-hexyl-phenyl side chains on the IDT unit and exhibits E_g^{opt} of 1.79 eV.[13] When condensed with an additional thiophene ring IDTT—a ladder-type electron-rich moiety—can be formed, which features improved mobility and absorption coefficients of its copolymers compared to IDT-based polymers.[7] Moreover, the weak donating strength of IDTT results in conjugated polymers with deep-lying HOMO levels, a parameter which should benefit oxidative stability and lead to high V_{oc} in photovoltaic devices. In fact, Jen et al. reported a D–A copolymer based on IDTT and difluoro-benzothiadiazole with a PCE of 7.7%, a V_{oc} close to 1 V and E_g^{opt} of 1.78 eV.[13]

One important aspect in a variety of D–A polymers is the correlation between the number-average molecular weight (M_n) of the polymer and its bulk heterojunction (BHJ) solar cell performance.[14–33] In some cases, by increasing M_n the efficiency of OPVs could be increased by a factor of 2.[17,24,33] Modest differences in M_n can lead to significant batch-to-batch variations and thus to differences in the performance of the same polymer when synthesized by different research groups.[4,5,34,35] It is, therefore, essential to investigate and understand the influence of M_n in newly developed conjugated polymers for OPVs. This goes along with the studies by You et al., who recently discussed that the "optimal" molecular weight can be polymer specific.[31] Common practice for controlling the molecular weight includes: i) the proper adjustment of the stoichiometric ratio between the initial reagents,[17,31,32] ii) the polymerization time,[19,22] and iii) the fractionation of the polymer samples through Soxhlet extraction[33] or preparative gel permeation chromatography (GPC).[30] While the correlation between molecular weight and J_{sc} and FF were discussed for several material classes,[30] the impact of the molecular weight on the radiative V_{oc} losses was only recently observed.[36]

In this work, we synthesized and investigated a new D–A high band gap conjugated polymer (PIDTTQ) as a function of M_n. The copolymer consists of indacenodithieno[2,3] thiophene as the electron-rich moiety and 2,3-bis(3-(octyloxy)phenyl)quinoxaline as the electron-deficient unit (Scheme 1). 2,3-Diphenylquinoxaline units have been shown to form efficient high band gap polymers when combined with IDT donor groups.[11] In the best case, the active material exhibits more than 6% PCE in inverted solar cells processed via doctor blading in air, without requiring thermal treatment.

The photovoltaic performance of this novel material depends strongly on the molecular weight. To study the optoelectronic characteristics of these new polymer systems as a function of M_n we combined photovoltaic device characterization with photoinduced charge carrier extraction by linear increasing voltage (photo-CELIV), and Fourier-transform photocurrent spectroscopy (FTPS) paired with electroluminescence spectroscopy (EL). We demonstrate that high molecular weight PIDTTQ yields higher photocurrent, fill factor, and efficiency mainly because of a) improved light absorption and charge carrier transport properties, and b) lower nonradiative recombination losses. Thus, this analysis shows that controlling polymer synthesis to yield high M_n is particularly critical for attaining low-loss photovoltaic and proper optoelectronic characteristics in PIDTT-quinoxaline-based bulk heterojunction devices.

2. Results and Discussion

The polymer PIDTTQ was synthesized by Stille aromatic cross-coupling polymerization[37] of a stoichiometric balance ratio of the distannyl derivative of *para*-hexyl-phenyl substituted IDTT and 5,8-dibromo-2,3-bis(3-(octyloxy)phenyl)quinoxaline in the presence of tris(dibenzylideneacetone)dipalladium(0) (Pd_2dba_3) and tri(*o*-tolyl)phosphine ($P(o\text{-}tol)_3$) as the catalytic system (Scheme 1).

To obtain the low molecular weight polymer (PIDTTQ-LMW, 20 kD), the polymerization was carried out in nondistilled toluene at 110 °C for 48 h. The medium molecular weight polymer (PIDTTQ-MMW, 40 kD), on the other hand, was prepared using anhydrous toluene at 120 °C for 36 h. When extending the duration of the polymerization to 48 h the molecular weight could be increased to 58 kD, forming the polymer PIDTTQ-HMW (see the Experimental Section for details). The GPC profiles relative to a polystyrene standard of synthesized PIDTTQ polymers shown in Figure S1a (Supporting Information) conspicuously reflect the difference in molecular weight. The estimated molecular weights are summarized in Table S1 (Supporting Information). We emphasize that while GPC measurements have proven useful to correctly identify trends of relative molecular weights GPC is equally known to overestimate the molecular weight by factors of up to 1.6.[31] Thermogravimetric analysis (TGA) of PIDTTQ-HMW under ambient conditions shows that the molecular structure of PIDTTQ-HMW remains intact up to 290 °C, demonstrating considerable thermal stability (Figure S1b, Supporting Information).

Table 1. Oxidation and reduction potentials of the synthesized PIDTTQ polymers.

M_n [kD]	$E_{ox,onset}$ [V] versus Ag/AgCl	$E_{red,onset}$ [V] versus Ag/AgCl	$E_{ox,onset}$ [V] versus Fc/Fc^+	$E_{red,onset}$ [V] versus Fc/Fc^+	E_{HOMO} [eV]	E_{LUMO} [eV]	E_g,ec [eV][a)]	E_g,opt [eV][b)]
58	0.68	−0.90	0.12	−1.46	−5.22	−3.64	1.58	1.77
40	0.71	−0.96	0.18	−1.49	−5.28	−3.61	1.67	1.77
20	0.71	−0.99	0.18	−1.52	−5.28	−3.58	1.70	1.79

HOMO-LUMO energy levels and band gap values were estimated from cyclic voltammetry (CV) data. [a)]Electrochemical band gap E_g,ec calculated from CV (HOMO-LUMO); [b)]Optical band gap calculated from UV–vis absorption onset.

The redox potentials of PIDTTQ with different M_n were investigated by cyclic voltammetry (CV; see the Experimental Section for details). The redox couple Fc/Fc^+ was used as reference redox potential. The voltagram traces featuring the reduction and oxidation potentials of PIDTTQ-HMW, PIDTTQ-MMW, and PIDTTQ-LMW in solution are shown in Figure S1c,d (Supporting Information). The resulting electrochemical energies of the frontier molecular orbitals as estimated by $E_{LUMO/HOMO} = -(5.1 + E_{on}^{red/ox})$ eV are summarized in **Table 1** (HOMO: highest occupied molecular orbital, LUMO: lowest unoccupied MO; $E_{on}^{red/ox}$: redox potential vs Fc/Fc^+). The oxidation potential from the onset is 0.68 V for PIDTTQ-HMW versus Ag/AgCl and 0.71 for PIDTTQ-MMW and PIDTTQ-LMW. The resulting oxidation onsets are 0.12 and 0.18 V versus Fc/Fc^+, leading to an estimated HOMO level (E_{HOMO}) of −5.22 eV for PIDTTQ-HMW and −5.28 eV for PIDTTQ-MMW and PIDTTQ-LMW. In addition, the reduction onsets versus Ag/AgCl were estimated to be −0.90, −0.96, and −0.99 V for PIDTTQ HMW, MMW, and LMW, respectively. The resulting E_{LUMO} levels of PIDTTQ-HMW, PIDTTQ-MMW, and PIDTTQ-LMW are −3.64, −3.61, and −3.58 eV, respectively. Overall, the CV measurements reveal that the LUMO level gradually shifts to deeper values versus vacuum as M_n increases, whereas the HOMO level of the low and medium M_n copolymers remains the same at low molecular weights and is upshifted versus vacuum as M_n further increases.

The thin film UV–vis absorption spectra of PIDTTQ for the three different M_n values, normalized by the film thickness, are shown in **Figure 1**b. All polymers depict two distinct absorption bands in the wavelength range of 350–450 and 500–700 nm, corresponding to a π–π^* transition and intramolecular charge transfer (ICT) between the IDTT and quinoxaline moieties, respectively.[12] While the absorption profile of PIDTTQ in the solid state does not change with molecular weight—only a slight blue shift of the low energy absorption band from 628 to 619 nm with increasing M_n is observed (Figures 1b and S3, Supporting Information)—it is apparent that the absorption coefficient increases with increasing molecular weight. The

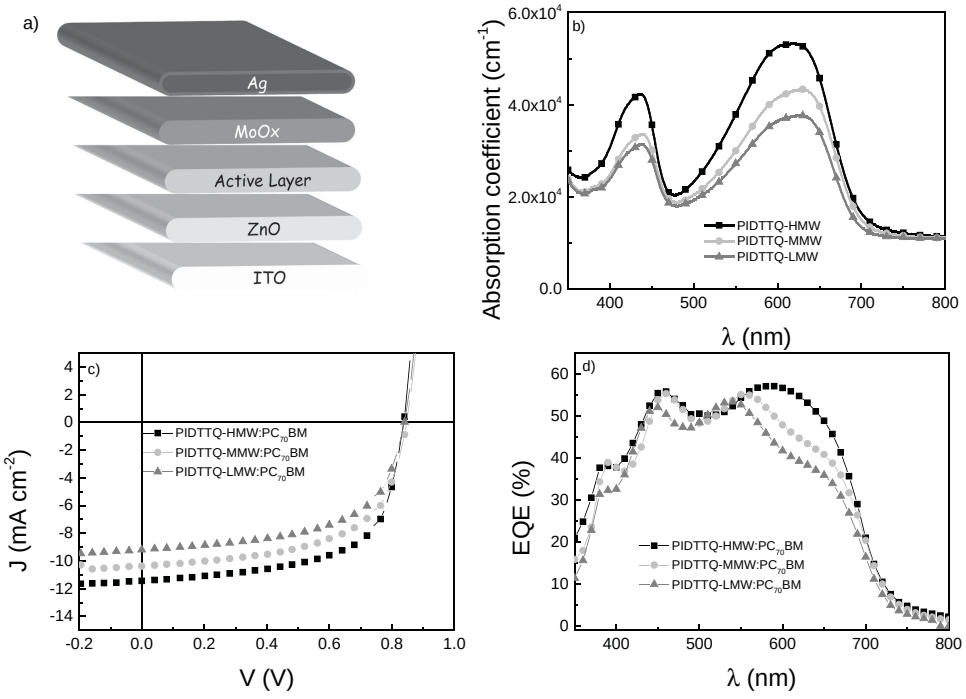

Figure 1. Photovoltaic performance of PIDTTQ-based solar cells. a) Schematic device representation of BHJ solar cells with the device layout ITO/ZnO/PIDTTQ:$PC_{70}BM$ (1:2 w/w)/MoO_x/Ag). b) Absorption spectra of the pristine PIDTTQ-HMW, PIDTTQ-MMW, and PIDTTQ-LMW polymers in thin films. c) Current density–voltage characteristics of PIDTTQ-HMW, PIDTTQ-MMW, and PIDTTQ-LMW-based solar cells under solar simulator illumination (100 mW cm^{-2}). d) External quantum efficiency curves of the same devices as shown in (c).

Table 2. Photovoltaic device parameters of low, medium, and high molecular weight PIDTTQ-based inverted solar cells under 1 sun illumination (100 mW cm^{-2}).

M_n [kD]	V_{oc} [V]	J_{sc} [mA cm^{-2}]	FF	η [%]
58	0.84 (0.84 ± 0.01)	11.45 (11.16 ± 0.19)	0.62 (0.61 ± 0.01)	6.01 (5.84 ± 0.16)
40	0.84 (0.84 ± 0.01)	10.37 (10.29 ± 0.10)	0.59 (0.58 ± 0.01)	5.25 (5.10 ± 0.20)
20	0.85 (0.84 ± 0.01)	9.19 (8.58 ± 0.65)	0.58 (0.57 ± 0.01)	4.53 (4.12 ± 0.33)

optical band gap (E_g^{opt}) in thin film, as measured by the absorption onset, does not vary noticeably with molecular weight and is 1.77–1.79 eV for all polymers (Figure 1b).

Next, we examined the BHJ solar cell performance of all three molecular weight fractions. All solar cells were fabricated using an inverted device structure consisting of ITO/ZnO[38]/PIDTTQ:$PC_{70}BM$ (1:2 w/w)/MoO_x/Ag (Figure 1a). The active layer solution was doctor bladed under ambient conditions using a 97 to 3 vol% mixture of 1,2-dichlorobenzene (*o*-DCB) and 1-chloronaphtalene (CN). CN is known to improve the morphology and thus enhance the performance of BHJ solar cells based on IDTT-type polymers.[12] Figures 1c and S4 (Supporting Information) show *J*–*V* curves of optimized BHJ solar cells under simulated AM1.5G solar irradiation (100 mW cm^{-2}) and in the dark, respectively.

The best performing solar cells were obtained using PIDTTQ-HMW, achieving a short circuit current density (J_{sc}) of 11.45 mA cm^{-2}, an open circuit voltage (V_{oc}) of 0.84 V, a fill factor (FF) of 0.62, and a PCE of 6.0%. The average efficiency of more than 30 devices was 5.8%. Using the same fabrication methodology, solar cells containing PIDTTQ-LMW and PIDTTQ-MMW achieved a maximum PCE of 4.5% and 5.3%, respectively, in the best case. As shown in **Table 2**, the main enhancement when increasing the molecular weight is reflected in J_{sc} and FF with only minor variations in V_{oc}. Noticeably, the rectification behavior of the devices improved with increasing molecular weight (Figure S4, Supporting Information).

We further measured external quantum efficiency (EQE) spectra of OPV devices made from PIDTTQ (Figure 1d). Photoaction spectra of active layers with increasing M_n show improved photoresponse particularly around 600 nm, i.e., the enhancement in J_{sc} originates dominantly from the polymer absorption regime. This result may suggest a more favorable polymer packaging and/or aggregation and, consequently, more efficient charge generation and collection in the case of PIDTTQ with high molecular weight. We note that the integrated EQE for these devices matches the measured short circuit current within a margin of 10%.

Indeed, the *J*–*V* characteristics show that the devices exhibit a clear trend with increasing M_n, not only in J_{sc}, but also in FF, where we found values of 0.58, 0.59, and 0.62 for M_n of 20, 40, 58 kD, respectively (Figure 1c). A strong correlation between photovoltaic parameters and average molecular weight per number, where higher M_n leads to higher PCE, has been reported for a variety of D–A polymer–fullerene systems.[17,30] However, the physical origin of such a correlation is not straightforward to identify. Previous reports suggested that differences in molecular weight may result in either an altered microstructure, a changed charge transport, and/or recombination mechanisms or in deviating the charge generation rate. To elucidate between these processes, we carried out a careful study of microstructural and photophysical properties.

We started our analysis by investigating the surface microstructure of the active layer through intermittent contact mode atomic force microscopy (AFM, Figure S5, Supporting Information). Interestingly, the topography features spherical, sub-100 nm domains, consistent with previous reports on IDTT-based polymers.[13] This striking motif is discernible for all polymer batches. While we cannot associate these domains with a particular component of the BHJ, the topography and phase images do not reveal obvious differences between the three systems studied. We emphasize that although UV–vis absorption and EQE point to a better polymer-chain organization with increasing M_n, this is not apparent from AFM data. We, therefore, performed transmission electron microscopy (TEM) investigations of the active layer films. **Figure 2** shows TEM bright field images as well as elemental maps based on energy filtered TEM (EFTEM) imaging of carbon (C) using the C K edge and of sulfur (S) using the S L edge. Because only PIDTTQ comprises sulfur and because of sufficient contrast in the elemental maps, we are able to distinguish between polymer and fullerene phases. The C signal is used to represent $PC_{70}BM$ because of the difference in the C content of $PC_{70}BM$ and PIDTTQ (C-$PC_{70}BM$ = 83.7 at% and C-PIDTTQ = 45.6 at%). In the case of PIDTTQ-LMW the formation of separated domains is clearly discernible. The domains of $PC_{70}BM$ have a diameter of about 100 nm. The size of the $PC_{70}BM$ domains decreases to about 50 nm in the case of PIDTTQ-MMW. In contrast, the PIDTTQ-HMW:$PC_{70}BM$ blend shows much finer intermixing of the polymer and the fullerene phases. Generally, the intermixing behavior revealed by TEM correlates well with the photovoltaic device performance, i.e., the smaller the domain sizes of the polymer and the fullerene, the better the device performance.

To examine the impact of M_n on charge generation, we measured the photocurrent density (J_{ph}) as a function of effective voltage (V_{eff}), as shown in **Figure 3**.[39] The measured photocurrent is defined as $J_{ph} = J_l - J_d$, where J_l and J_d are the current density under illumination at 100 mW cm^{-2} and in the dark, respectively. V_{eff} is given by $V_{eff} = V_0 - V$, where V_0 is the compensation voltage defined as $J_{ph}(V_0) = 0$, and V is the applied voltage. The *J*–*V* plots indicate that J_{ph} quickly saturates for $V_{eff} > 1$ V. At full saturation, we can assume that all generated electron–hole pairs are dissociated and collected at the electrodes. This allows us to estimate the maximum generation rate of free charge carriers G_{max} according to $J_{sat} = qG_{max}L$,[40] where q is the electronic charge and L is the active layer thickness. Importantly, G_{max} is influenced significantly by M_n and values of 6.72×10^{21}, 7.18×10^{21}, and 7.59×10^{21} cm^{-3} s^{-1} can be extracted for polymers with M_n of 20, 40, and 58 kD, respectively (**Table 3**). The same trend is also observed when considering charge generation at the voltage V_{MPP} (MPP: maximum power point of *J*–*V* curve) and under short-circuit conditions ($V = 0$). For instance, at $V = 0$ and $V = V_{MPP}$ the charge generation rate achieved 94% and 76% of G_{max}, respectively, for M_n = 58 kD compared to 81% and 44% for M_n = 20 kD (Table 2).

The trend observed for G_{max} versus M_n is consistent with the enhancement of J_{sc} as well as the UV–vis absorption coefficient, indicating more efficient exciton generation and

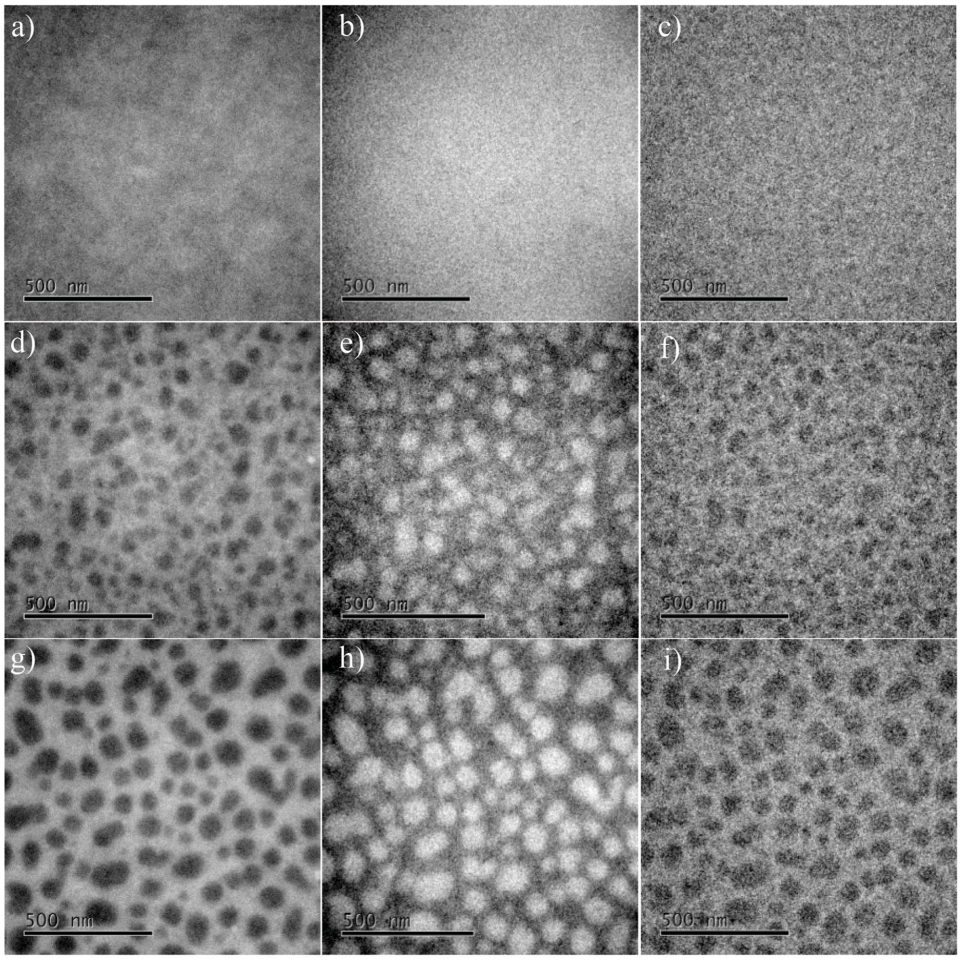

Figure 2. TEM bright field images (left column) and elemental maps based on energy filtered TEM (EFTEM) imaging of carbon (C K edge, center column) and of sulfur (S L edge, right column). a–c) PIDTTQ-HMW, d–f) PIDTTQ-MMW, and g–i) PIDTTQ-LMW. All polymers were blended with $PC_{70}BM$ (1:2). The scale bar represents 500 nm in all images.

separation with increasing molecular weight.[33,41] Note that we did not observe a square-root dependence of J_{ph} versus V_{eff} for PIDTTQ-HMW-based solar cells in any range of the effective voltage, therefore, excluding a space-charge effect or extraction limitation because of low mobility–lifetime ($\mu\tau$) product for these devices. However, a square-root regime of J_{ph} was observed for PIDTTQ-MMW and PIDTTQ-LMW polymers before saturation (Figure 3). To discern between the two limiting processes at low effective voltages, we measured photocurrent versus V_{eff} as a function of light intensity. The results are shown in Figure S6 (Supporting Information) for PIDTTQ-HMW, PIDTTQ-MMW, and PIDTTQ-LMW-based solar cells in dual logarithmic representation. The slope of J_{ph} as a function of P_{in} at low (0.1 V) and high (3 V) effective voltage is close to 1, suggesting that the main limitation is in fact because of a low $\mu\tau$ product.[42]

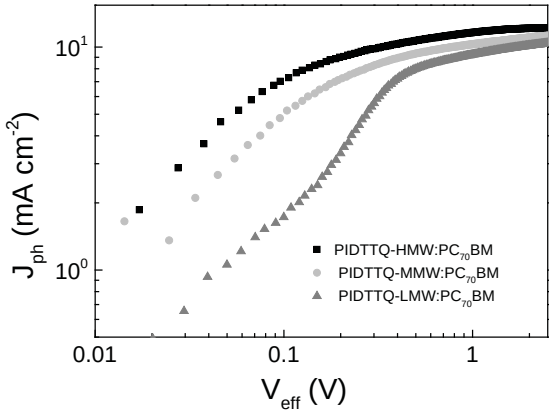

Figure 3. Photocurrent density of PIDTTQ-HMW, PIDTTQ-MMW, and PIDTTQ-LMW-based solar cells as a function of the effective voltage under 1 sun illumination.

As such, to understand the implications of M_n on $\mu\tau$ in more detail, we first investigated the charge carrier mobility μ of devices comprising the three different molecular weight polymers by employing the technique of photoinduced charge carrier extraction by linearly increasing voltage (photo-CELIV).[43] Charges are photogenerated by a strongly absorbed laser pulse and extracted after an adjustable delay time (Figure S7, Supporting Information). **Figure 4** shows the photo-CELIV transients of the three systems, which were recorded by applying

Table 3. Summary of calculated charge generation and charge transport parameters: saturation current (J_{sat}); maximum rate of free charge carrier generation in saturation regime (G_{MAX}), under maximum power point (G_{MPP}), and under short circuit conditions (G_{sc}); bimolecular charge carrier lifetime (τ) and mobility–lifetime product ($\mu\tau$) of PIDTTQ-HMW, PIDTTQ-MMW, and PIDTTQ-LMW-based devices.

M_n [kD]	J_{sat} [mA cm^{-2}]	G_{MAX} [cm^{-3} s^{-1}]	G_{MPP} [%]	G_{sc} [%]	μ [cm^2 V^{-1} s^{-1}]	τ [s]	$\mu\tau$ [cm^2 s^{-1}]
58	12.14	7.59×10^{21}	75.78	94.35	$(2.1\pm0.3)\times10^{-4}$	4.86×10^{-5}	1.02×10^{-8}
40	11.15	7.18×10^{21}	68.25	87.81	$(1.2\pm0.2)\times10^{-4}$	4.12×10^{-5}	4.95×10^{-9}
20	10.75	6.72×10^{21}	43.97	80.86	$(7.2\pm0.5)\times10^{-5}$	2.10×10^{-5}	1.51×10^{-9}

a 2 V/20 µs linearly increasing reverse bias pulse and a delay time (t_d) of 1 µs. From the measured photocurrent transients, the charge carrier mobility (μ) is calculated using the following Equation (1):

$$\mu = \frac{2d^2}{3At_{max}^2\left[1+0.36\frac{\Delta j}{j(0)}\right]} \text{ if } \Delta j \le j(0) \quad (1)$$

where d is the active layer thickness, A is the voltage rise speed $A = \mathrm{d}U/\mathrm{d}t$ U is the applied voltage, t_{max} is the time corresponding to the maximum of the extraction peak, and $j(0)$ is the displacement current.[44] The photocurrent transients in Figure 4 reveal that t_{max} occurs significantly earlier for higher M_n. As a result, the calculated charge carrier mobility increases with increasing M_n and amounts to $(2.1\pm0.2)\times10^{-4}$ $(1.1\pm0.2)\times10^{-4}$, and $(7.2\pm0.5)\times10^{-5}$ cm^2 V^{-1} s^{-1} for PIDTTQ-HMW, PIDTTQ-MMW, and PIDTTQ-LMW solar cells, respectively. The dependence of the charge carrier mobility on M_n correlates with the photovoltaic efficiency. A higher charge carrier mobility certainly contributes to an improved extraction behavior and consequently to a higher PV performance.

We then analyzed the lifetime t of the charge carrier density. As shown in Figure S8 (Supporting Information), the number of collected charge carriers decreases with increasing delay time between photogeneration and extraction because of recombination losses inside the device. Under the present conditions, the decay in carrier population can be fitted using a time-dependent, bimolecular recombination kinetics model.[43]

$$\frac{\mathrm{d}n}{\mathrm{d}t} = -\beta(t)n^2 \quad (2)$$

where $\beta(t)$ is the time-dependent recombination coefficient. Assuming a power-law decay of the shape $\beta(t) = \beta_0 t\exp(-(1-\gamma))$ where β_0 and γ are time-independent parameters, the following analytical solution of Equation (2) can be derived:[43]

$$n(t) = \frac{n(0)}{1+\left(\frac{t}{T_B}\right)^{\gamma}} \quad (3)$$

where $n(0)$ is the density of photogenerated carriers at $t = 0$ and T_B is the bimolecular lifetime. By fitting the curves of Figure S8 (Supporting Information) with Equation (3), we can estimate $n(0)$ to be 5.89×10^{14}, 5.42×10^{14}, and 5.26×10^{14} cm^{-3} and T_B to be 4.86×10^{-5}, 4.12×10^{-5}, and 2.10×10^{-5} s for PIDTTQ-HMW, PIDTTQ-MMW, and PIDTTQ-LMW solar cells, respectively (Table 3). Thus, the PIDTTQ-HMW:PC$_{70}$BM device not only shows the highest charge carrier mobility but also the highest initial density of photogenerated carriers and highest bimolecular lifetime among all polymer batches, which is consistent with the highest observed FF. As shown in the inset of Figure 4, the $\mu\tau$ product increases from 1.51×10^{-9} cm^2 V^{-1} to 4.95×10^{-9} and 1.02×10^{-8} cm^2 V^{-1} with increasing M_n. Overall, bimolecular recombination in the case of PIDTTQ-MMW and PIDTTQ-LMW-based OPVs originates from low charge carrier extraction because of $\mu\tau$-product limitation.

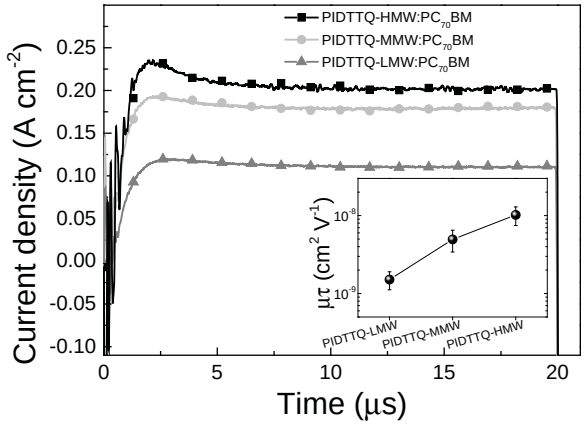

Figure 4. Time-dependent photo-CELIV traces of PIDTTQ-HMW, PIDTTQ-MMW, and PIDTTQ-LMW-based solar cells at a fixed delay time of 1 µs. t_{max} occurs at 3.10, 2.70, and 2.04 µs for 20, 40, and 58 kD polymers, respectively. The inset shows the mobility–lifetime product as a function of molecular weight.

While G_{max} and $\mu\tau$ product can explain the trend observed for J_{sc} and FF, respectively, elucidating the loss mechanisms associated with V_{oc} when controlling the molecular weight of a polymer is equally important. Therefore, we investigated first the radiative open circuit voltage V_0^{rad}, which represents the maximum achievable V_{oc}, as given by[45]

$$V_0^{rad} = \frac{kT}{q}\ln\left(\frac{J_{sc}}{J_0^{rad}}+1\right) \quad (4)$$

where kT/q is the thermal voltage and J_0^{rad} is the saturation current density. Afterward, based on the radiative open circuit voltage V_0^{rad} in Equation (4), we calculated the nonradiative recombination losses (ΔV_{oc}) according to[45,46]

$$\Delta V_{oc} = V_0^{rad} - V_{oc} \quad (5)$$

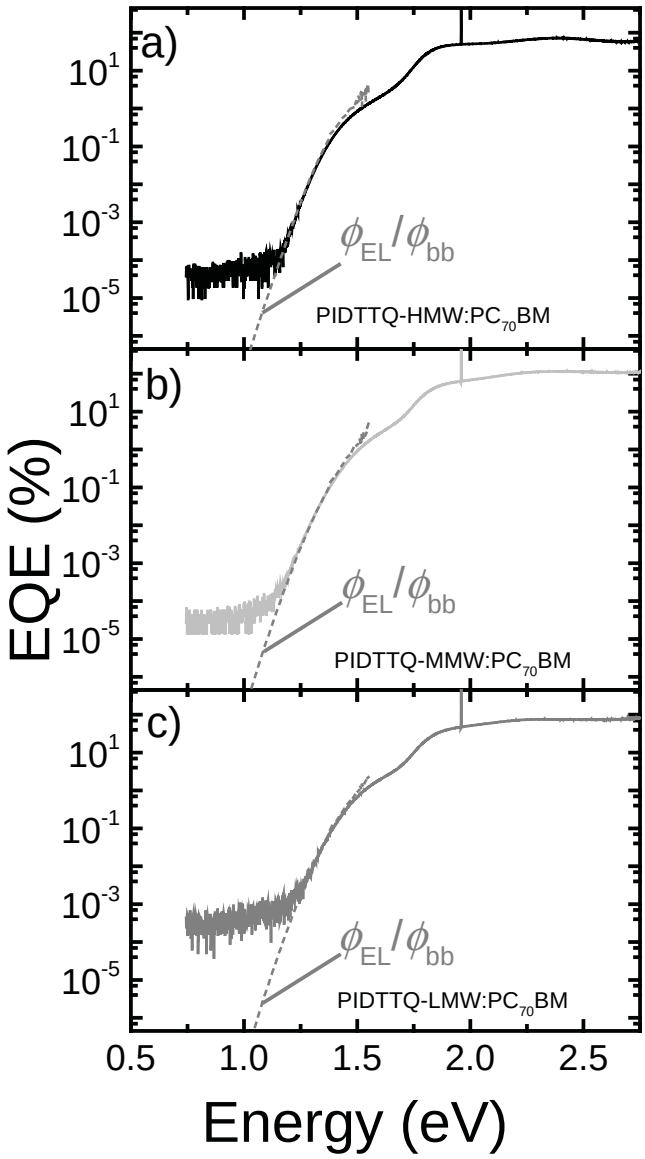

Figure 5. Semilogarithmic plots of the external quantum efficiency (EQE) as measured by Fourier-transform photocurrent spectroscopy FTPS (solid lines) and electroluminescence (EL) spectroscopy for solar cells based on PIDTTQ-HMW a), PIDTTQ-MMW b), and PIDTTQ-LMW c). The emitted spectral photon density $\phi_{\theta m}$ originating from EL was normalized by the spectral photon density of a black body ϕ_{bb}, giving rise to ϕ_{EL}/ϕ_{bb} (dashed lines).

In order to assess V_0^{rad} the saturation current density J_0^{rad} can be calculated from the external quantum efficiency by combining FTPS and EL measurements (see the Supporting Information for details).[45,46] **Figure 5** depicts FTPS and EL data for devices made from blends of PIDTTQ with $PC_{70}BM$, using the same device geometry as for the solar cells. Note that to match EL and FTPS spectra the emitted spectral photon density $\phi_{\theta m}$ as measured by EL needs to be normalized by the spectral photon density of a black body ϕ_{bb}.[45,46] **Table 4** summarizes the calculated values obtained from EL and FTPS measurements for PIDTTQ:$PC_{70}BM$-based solar cells. The radiative open circuit voltage V_0^{rad} is 1051, 1053, and 1121 mV for PIDTTQ-HMW, PIDTTQ-MMW, and PIDTTQ-LMW, respectively. Conversely, the nonradiative losses in open circuit voltage as calculated from Equation (5) are 330, 332, and 390 mV for PIDTTQ-HMW, PIDTTQ-MMW, and PIDTTQ-LMW, respectively. Importantly, the calculated losses are consistent with the results from the charge transport investigation: devices based on PIDTTQ-HMW with the best transport characteristics reveal the lowest V_{oc} losses, underlining the importance of molecular weight on nonradiative recombination pathways.

Table 4. Open circuit voltage (V_{oc}), current density (J_{sc}), radiative V_{oc} (V_{oc},^{rad}), radiative current density (J_0^{rad}), and loss (ΔV_{oc}) in PIDTTQ-HMW, PIDTTQ-MMW, and PIDTTQ-LMW devices.

M_n [kD]	V_{oc} [mV]	J_{sc} [mA cm^{-2}]	V_{oc},^{rad} [mV]	J_0^{rad} [mA cm^{-2}]	ΔV_{oc} [mV]
58	840	11.45	1051	2.51×10^{-20}	330
40	840	10.37	1053	2.12×10^{-20}	332
20	850	9.19	1121	1.36×10^{-20}	390

3. Conclusion

We synthesized a high band gap indacenodithieno[2,3] thiophene and quinoxaline-based semiconducting polymer by Stille polymerization and showed that controlling the number-average molecular weight M_n is particularly critical for attaining superior photovoltaic function in polymer–fullerene bulk heterojunction solar cells. Using photovoltaic and opto-electrical device characterization, we observed strong correlations between M_n and photovoltaic performance, charge generation, and charge transport. Specifically, polymers with low molar mass suffer from reduced probability of charge carrier generation, leading to lower short-circuit current, and $\mu\tau$-limited charge carrier extraction, in agreement with diminished fill factors.

The combination of UV–vis absorption, EQE, charge carrier lifetime, and photocurrent measurements suggest that the dominant loss may arise from shallow traps or defect states. These states seem to extend from the edge of the band gap just slightly into the band gap, causing scattering of the charge carriers, leading to reduced mobility and, eventually, higher order recombination.[47] Further, these states may explain our observed reduction in charge carrier generation rate in the case of low M_n, as the primary excitation may relax down to these states before finding a suitable fullerene to transfer the charge.

Crucially, we found that Fourier-transform photocurrent spectroscopy paired with electroluminescence spectroscopy provides evidence for energetic losses induced by the molecular structure. High molar mass polymers featuring higher carrier mobility exhibit less nonradiative recombination pathways for charge carriers, which is consistent with our transport observations.

Overall, the synthesis of PIDTTQ represents a versatile and reproducible route toward air-processable and efficient high band gap polymers, which could be scaled up for large area processing techniques of single and tandem polymer solar cells. While structure–property relations established in this work may

contribute to shaping the rational design of high-performance semiconducting OPV polymers, further investigations on the implications of molecular structure on device physics are necessary. Recently, Li et al.[31] demonstrated differences in device performance not only related to absolute molecular weight but also polydispersity. In order to gain a better understanding of the microscopic phenomena limiting the photovoltaic operation of conjugated OPV polymers control of both molecular weight and polydispersity will be a future challenge of polymer synthesis.

4. Experimental Section

All reactions were performed under argon atmosphere and in the dark. All glassware was cleaned using Teepol surfactant, rinsed with excess water, acetone, and methylene dichloride, and dried in an oven at 120 °C. All solvents and reagents were purchased from Sigma-Aldrich. The synthesis of 5,8-dibromo-2,3-bis(3-(octyloxy)phenyl)quinoxaline[48] and bis(trimethylstannyl)indacenodithieno[2,3] thiophene[7] were performed according to the previously reported literature.

Synthesis: Distannyl substituted *para*-hexyl-phenyl substituted IDTT (0.5 mmol, 204.88 mg) and 5,8-dibromo-2,3-bis(3-(octyloxy)-phenyl)quinoxaline (0.5 mmol, 348.29 mg) were dissolved in dry toluene (25 mL). Then, tris(dibenzylideneacetone)dipalladium(0) (Pd_2dba_3) (0.01 mmol, 9.16 mg) and tri(*o*-tolyl)phosphine ($P(o\text{-tol})_3$) (0.04 mmol, 12.17 mg) were added and the reaction mixture was stirred at 120 °C under argon atmosphere for 48 h. The polymer was purified by precipitation in acetone, filtered and washed using a Soxhlet apparatus with methanol, acetone, hexane, and chloroform. The chloroform fraction was evaporated under reduced pressure and the polymer was precipitated in acetone, filtered through 0.45 mm PTFE filter and finally dried under high vacuum, rendering a dark blue solid with metallic appearance and 88% of yield. The GPC profile and the ^{1}H-NMR and ^{13}C-NMR are presented in Figures S1 and S10 (Supporting Information), respectively. A similar synthetic procedure was followed for the preparation of PIDTTQ-MMW (83% yield) and PIDTTQ-LMW (86%) with slight modifications: PIDTTQ-MMW was stirred at 120 °C for 36 h while PIDTTQ-LMW was stirred at 110 °C for 48 h using nondistilled toluene.

Fabrication of Photovoltaic Devices: All devices were fabricated using doctor-blading under ambient conditions with the structure of Figure 1a. Prestructured indium tin oxide (ITO) substrates were cleaned with acetone and isopropyl alcohol in an ultrasonic bath for 10 min each. After drying, the substrates were successively coated with 40 nm of zinc oxide (ZnO), 10 nm of $Ba(OH)_2$, and finally a 80–90 nm thick active layer based on PIDTTQ:$PC_{70}BM$ (20 g L^{-1}). To complete the fabrication of the devices 10 nm of MoOx and 100 nm of Ag were thermally evaporated through a mask (with a 10.4 mm^2 active area opening) under a vacuum of $\approx 5 \times 10^{-6}$ mbar.

Gel Permeation Chromatography (GPC): GPC was equipped with an isocratic pump (Spectra System P1000), three columns in series (PLgel 5 mm Mixed-C, 300 × 7.5 mm), a refractive index (RI, Shodex RI-101) detector, and THF as the eluent at a flow rate of 1 mL min^{-1}.[49] It should be noted that the eluent included ≈2% v/v triethylamine in order to exclude any retention effect inside the columns because of polar additives, if any. Polystyrene standards (M_p: 4300–3 000 000 g mol^{-1}) were used for the calibration of the instrument.

Nuclear Magnetic Resonance (NMR): ^{1}H-NMR and ^{13}C-NMR measurements were carried out in solutions (1% w/v) of the copolymers using $CDCl_3$ (Acros 99.6%) as the solvent and tetramethylsilane (TMS) as the integral standard on a Brucker AV-250 spectrometer using a resonance frequency of ^{1}H-250 MHz. The NMR system was controlled by TopSpin 2.1 software by Bruker. (Figure S9, Supporting Information).

Thermogravimetric Analysis (TGA): TGA measurements were performed on a Perkin-Elmer Pyris Diamond TG/DTA. Samples of approximately 5 mg were heated in air from 25 to 900 °C, at a rate of 5 °C min^{-1}.

Cyclic Voltammetry (CV): CV studies were performed using a standard three-electrode cell. A platinum disk electrode was used as a working electrode, a platinum wire as the counter-electrode, and silver/silver chloride (Ag/AgCl) as the reference electrode. Tetrabutylammonium hexafluorophosphate ($TBAPF_6$; 98%) was used as an electrolyte. It was recrystallized three times from acetone and dried in a vacuum at 100 °C prior to each experiment. Measurements were recorded using an Autolab EcoChemie potensiostat/galvanostat Model PGSTAT10, which was connected to a personal computer running General Purpose Electrochemical System software version 4.9. In a typical experiment, 2–5 mg of the material was diluted in a mixture of *o*-DCB/acetonitrile (4:1 by volume) in the presence of 0.1 M $TBAPF_6$. The cyclic voltammetry graphs were recorded at a potential scan rate of 50 mV s^{-1} under nitrogen atmosphere. The oxidation and reduction potentials were calibrated against a ferrocene/ferrocenium (Fc/Fc^+) redox couple.

J–V Measurements: The *J–V* characteristics were measured using a source measurement unit from BoTest. Illumination was provided by a solar simulator (Oriel Sol 1A, from Newport) with AM1.5G spectrum at 100 mW cm^{-2}. UV–vis absorption was performed on a Lambda 950 from Perkin-Elmer. EQEs were measured using an integrated system from Enlitech, Taiwan. In order to study the light intensity dependence of current density, we used a series of neutral color density filters. The intensity of light transmitted through the filter was independently measured via a power meter. All the devices were tested in ambient air.

Photo-CELIV: In photo-CELIV measurements, the devices were illuminated with a 405 nm laser diode. Current transients were recorded across an internal 50 Ω resistor of an oscilloscope (Agilent Technologies DSO-X 2024A). A fast electrical switch was used to isolate the cell and prevent charge extraction or sweep out during the laser pulse and the delay time. After a variable delay time, a linear extraction ramp was applied via a function generator. The ramp, which was 20 µs long and 2 V in amplitude, was set to start with an offset matching the V_{oc} of the cell for each delay time.

FTPS: FTPS-EQE was carried out using a modified Vertex 70 FTIR spectrometer from Brucker optics, equipped with QTH lamp, quartz beam splitter, and external detector. A low noise current amplifier (Femto, DLPCA-200) was used to amplify the photocurrent produced upon illumination of the photovoltaic device with light modulated by the FTIR. The output voltage of the current amplifier was fed back to the external detector port of the FTIR in order to be able to use the FTIR's software to collect the photocurrent spectrum.

EL: EL measurements were performed by using a chopper and applying a constant current (100 mA cm^{-2}) supplied by an external current/voltage source through the devices which have an active area of 0.104 cm^2. The emitted light was then collected by a monochromator and detected by a liquid-nitrogen-cooled InGaAs detector. The spectrum was recorded by a standard lock-in technique. The system was wavelength calibrated.

AFM: AFM measurements were performed on a solver nano from NT-MDT using 300 kHz single-crystal silicon cantilevers (Nt-MDT, NSG30).

TEM: The active layers for the TEM investigations were prepared as plan view specimens. Therefore, films of PEDOT:PSS and PIDTTQ:$PC_{70}BM$ with a thickness of 50 nm were deposited on glass using doctor-blading under ambient conditions. To float off the active layer, the sample was put into a vessel with distilled water, where PEDOT:PSS dissolved, and the active layer was transferred to a Cu TEM supporting grid. The TEM investigations were performed using an FEI Titan Themis^3 300 TEM with a high brightness field emission gun (X-FEG) operated at 200 kV equipped with a high-resolution Gatan imaging filter (GIF Quantum) used for electron energy-loss spectroscopy (EELS) and energy filtered TEM (EFTEM). Elemental maps were calculated using the three-window-technique.

Supporting Information

Supporting Information is available from the Wiley Online Library or from the author.

Acknowledgements

This project was funded by the European Community's Seventh Framework Programme (FP7/2007-2013) under the Grant Agreement no. 607585 project OSNIRO. C.L.C. acknowledges the financial support of a Marie Curie Intra European Fellowship (FP7-PEOPLE-2012-IEF) Project ECOCHEM. M.S. acknowledges primary support from a fellowship by the Portuguese Fundação para a Ciência e a Tecnologia (SFRH/BPD/71816/2010). The authors gratefully acknowledge the support of the Cluster of Excellence "Engineering of Advanced Materials" at the University of Erlangen-Nuremberg, which is funded by the German Research Foundation (DFG) within the framework of its "Excellence Initiative," Synthetic Carbon Allotropes (SFB953), and Solar Technologies go Hybrid (SolTech).
Note: Units of μs in the caption of Figure 4 were corrected on August 12, 2015.

Received: March 17, 2015
Revised: May 29, 2015
Published online: June 26, 2015

[1] a) T. Ameri, N. Li, C. J. Brabec, *Energy Environ. Sci.* **2013**, *6*, 2390; b) J. You, L. Dou, K. Yoshimura, T. Kato, K. Ohya, T. Moriarty, K. Emery, C.-C. Chen, J. Gao, G. Li, Y. Yang, *Nat. Commun.* **2013**, *4*, 1446; c) L. Dou, J. You, J. Yang, C.-C. Chen, Y. He, S. Murase, T. Moriarty, K. Emery, G. Li, Y. Yang, *Nat. Photonics* **2012**, *6*, 180; d) Y. Zhou, C. Fuentes-Hernandez, J. W. Shim, T. M. Khan, B. Kippelen, *Energy Environ. Sci.* **2012**, *5*, 9827; e) Y. Dong, X. Hu, C. Duan, P. Liu, S. Liu, L. Lan, D. Chen, L. Ying, S. Su, X. Gong, F. Huang, Y. Cao, *Adv. Mater.* **2013**, *25*, 3683; f) X. Guo, N. Zhou, S. J. Lou, J. Smith, D. B. Ticel, J. W. Hennek, R. P. Ortiz, J. T. L. Navarrete, S. Li, J. Strzalka, L. X. Chen, R. P. H. Chang, A. Facchetti, T. J. Marks, *Nat. Photon.* **2013**, *7*, 825; g) C. E. Small, S. Chen, J. Subbiah, C. M. Amb, S. W. Tsang, T. H. Lai, J. R. Reynolds, F. So, *Nat. Photonics* **2012**, *6*, 115; h) C. L. Chochos, S. A. Choulis, *Prog. Polym. Sci.* **2011**, *36*, 1326.

[2] S. C. Price, A. C. Stuart, L. Yang, H. Zhou, W. You, *J. Am. Chem. Soc.* **2011**, *133*, 4625.

[3] E. Wang, L. Hou, Z. Wang, S. Hellström, F. Zhang, O. Inganäs, M. R. Andersson, *Adv. Mater.* **2010**, *22*, 5240.

[4] C. Piliego, T. W. Holcombe, J. D. Douglas, C. H. Woo, P. M. Beaujuge, J. M. J. Fréchet, *J. Am. Chem. Soc.* **2010**, *132*, 7595.

[5] Y. Zou, A. Najari, P. Berrouard, S. Beaupré, B.-R. Aïch, Y. Tao, M. Leclerc, *J. Am. Chem. Soc.* **2010**, *132*, 5330.

[6] M. C. Yuan, M. Y. Chiu, S. P. Liu, C. M. Chen, K. H. Wei, *Macromolecules* **2010**, *43*, 6936.

[7] Y.-X. Xu, C.-C. Chueh, H.-L. Yip, F.-Z. Ding, Y.-X. Li, C.-Z. Li, X. Li, W.-C. Chen, A. K.-Y. Jen, *Adv. Mater.* **2012**, *24*, 6356.

[8] H. Zhong, Z. Li, F. Deledalle, E. C. Fregoso, M. Shahid, Z. Fei, C. B. Nielsen, N. Yaacobi-Gross, S. Rossbauer, T. D. Anthopoulos, J. R. Durrant, M. Heeney, *J. Am. Chem. Soc.* **2013**, *135*, 2040.

[9] N. Li, D. Baran, K. Forberich, F. Machui, T. Ameri, M. Turbiez, M. Carrasco-Orozco, M. Drees, A. Facchetti, F. C. Krebs, C. J. Brabec, *Energy Environ. Sci.* **2013**, *6*, 3407.

[10] M. T. Lloyd, D. C. Olson, P. Lu, E. Fang, D. L. Moore, M. S. White, M. O. Reese, D. S. Ginley, J. W. P. Hsu, *J. Mater. Chem.* **2009**, *19*, 7638.

[11] a) S.-H. Chan, C.-P. Chen, T.-C. Chao, C. Ting, C.-S. Lin, B.-T. Ko, *Macromolecules* **2008**, *41*, 5519; b) C.-P. Chen, S.-H. Chan, T.-C. Chao, C. Ting, B.-T. Ko, *J. Am. Chem. Soc.* **2008**, *130*, 12828; c) C.-Y. Yu, C.-P. Chen, S.-H. Chan, G.-W. Hwang, C. Ting, *Chem. Mater.* **2009**, *21*, 3262; d) Y.-C. Chen, C.-Y. Yu, Y.-L. Fan, L.-I. Hung, C.-P. Chen, C. Ting, *Chem. Commun.* **2010**, *46*, 6503; e) Y. Zhang, J. Zou, H.-L. Yip, K.-S. Chen, J. A. Davies, Y. Sun, A. K.-Y. Jen, *Macromolecules* **2011**, *44*, 4752; f) Y. Zhang, S.-C. Chien, K.-S. Chen, H.-L. Yip, Y. Sun, J. A. Davies, F.-C. Chen, A. K.-Y. Jen, *Chem. Commun.* **2011**, *47*, 11026; g) Y. Sun, S.-C. Chien, H.-L. Yip, Y. Zhang, K.-S. Chen, D. F. Zeigler, F.-C. Chen, B. Lin, A. K.-Y. Jen, *J. Mater. Chem.* **2011**, *21*, 13247; h) Y. Zhang, J. Zou, H.-L. Yip, K.-S. Chen, D. F. Zeigler, Y. Sun, A. K.-Y. Jen, *Chem. Mater.* **2011**, *23*, 2289; i) Y.-X. Xu, C.-C. Chueh, H.-L. Yip, C.-Y. Chang, P.-W. Liang, J. J. Intemann, W.-C. Chen, A. K.-Y. Jen, *Polym. Chem.* **2013**, *4*, 5220; j) Y. Xia, Y. Gao, Y. Zhang, J. Tong, J. Li, H. Li, D. Chen, D. Fan, *Polymer* **2013**, *54*, 607; k) M. Wang, X. Hu, L. Liu, C. Duan, P. Liu, L. Ying, F. Huang, Y. Cao, *Macromolecules* **2013**, *46*, 3950; l) R. He, L. Yu, P. Cai, F. Peng, J. Xu, L. Ying, J. Chen, W. Yang, Y. Cao, *Macromolecules* **2014**, *47*, 2921.

[12] K. Yao, M. Salvador, C.-C. Chueh, X.-K. Xin, Y.-X. Xu, D. W. deQuilettes, T. Hu, Y. Chen, D. S. Ginger, A. K.-Y. Jen, *Adv. Energy Mater.* **2014**, *4*, 1400206.

[13] D. Dang, W. Chen, S. Himmelberger, Q. Tao, A. Lundin, R. Yang, W. Zhu, A. Salleo, C. Müller, E. Wang, *Adv. Energy Mater.* **2014**, *4*, 1400680.

[14] P. Schilinsky, U. Asawapirom, U. Scherf, M. Biele, C. J. Brabec, *Chem. Mater.* **2005**, *17*, 2175.

[15] R. J. Kline, M. D. McGehee, E. N. Kadnikova, J. Liu, J. M. J. Fréchet, M. F. Toney, *Macromolecules* **2005**, *38*, 3312.

[16] W. Ma, J. Y. Kim, K. Lee, A. J. Heeger, *Macromol. Rapid Commun.* **2007**, *28*, 1776.

[17] R. C. Coffin, J. Peet, J. Rogers, G. C. Bazan, *Nat. Chem.* **2009**, *1*, 657.

[18] D. J. D. Moet, M. Lenes, J. D. Kotlarski, S. C. Veenstra, J. Sweelssen, M. M. Koetse, B. de Boer, P. W. M. Blom, *Org. Electron.* **2009**, *10*, 1275.

[19] S. Wakim, S. Beaupré, N. Blouin, B.-R. Aich, S. Rodman, R. Gaudiana, Y. Tao, M. Leclerc, *J. Mater. Chem.* **2009**, *19*, 5351.

[20] J. C. Bijleveld, A. P. Zoombelt, S. G. J. Mathijssen, M. M. Wienk, M. Turbiez, D. M. de Leeuw, R. A. J. Janssen, *J. Am. Chem. Soc.* **2009**, *131*, 16616.

[21] M. Tong, S. Cho, J. T. Rogers, K. Schmidt, B. B. Y. Hsu, D. Moses, R. C. Coffin, E. J. Kramer, G. C. Bazan, A. J. Heeger, *Adv. Funct. Mater.* **2010**, *20*, 3959.

[22] C. Müller, E. Wang, L. M. Andersson, K. Tvingstedt, Y. Zhou, M. R. Andersson, O. Inganäs, *Adv. Funct. Mater.* **2010**, *20*, 2124.

[23] J.-H. Huang, F.-C. Chen, C.-L. Chen, A. T. Huang, Y.-S. Hsiao, C.-M. Teng, F.-W. Yen, P. Chen, C.-W. Chu, *Org. Electron.* **2011**, *12*, 1755.

[24] I. Osaka, M. Saito, H. Mori, T. Koganezawa, K. Takimiya, *Adv. Mater.* **2011**, *24*, 425.

[25] X. Zhao, H. Tang, D. Yang, H. Li, W. Xu, L. Yin, X. Yang, *Chin. J. Chem.* **2012**, *30*, 2052.

[26] B. R. Aïch, J. Lu, S. Beaupré, M. Leclerc, Y. Tao, *Org. Electron.* **2012**, *13*, 1736.

[27] W. Li, W. S. C. Roelofs, M. M. Wienk, R. A. J. Janssen, *J. Am. Chem. Soc.* **2012**, *134*, 13787.

[28] W. Li, K. H. Hendriks, W. S. C. Roelofs, Y. Kim, M. M. Wienk, R. A. J. Janssen, *Adv. Mater.* **2013**, *25*, 3182.

[29] K. H. Hendriks, G. H. L. Heintges, V. S. Gevaerts, M. M. Wienk, R. A. J. Janssen, *Angew. Chem. Int. Ed.* **2013**, *52*, 8341.

[30] R. S. Ashraf, B. C. Schroeder, H. A. Bronstein, Z. Huang, S. Thomas, R. Joseph Kline, C. J. Brabec, P. Rannou, T. D. Anthopoulos, J. R. Durrant, I. McCulloch, *Adv. Mater.* **2013**, *25*, 2029.

[31] W. Li, L. Yang, J. R. Tumbleston, L. Yan, H. Ade, W. You, *Adv. Mater.* **2014**, *26*, 4456.
[32] J. A. Bartelt, J. D. Douglas, W. R. Mateker, A. El Labban, C. J. Tassone, M. F. Toney, J. M. J. Fréchet, P. M. Beaujuge, M. D. McGehee, *Adv. Energy Mater.* **2014**, *4*, 1301733.
[33] T.-Y. Chu, J. Lu, S. Beaupré, Y. Zhang, J.-R. Pouliot, J. Zhou, A. Najari, M. Leclerc, Y. Tao, *Adv. Funct. Mater.* **2012**, *22*, 2345.
[34] Y. Zhang, S. K. Hau, H.-L. Yip, Y. Sun, O. Acton, A. K.-Y. Jen, *Chem. Mater.* **2010**, *22*, 2696.
[35] C. Cabanetos, A. El Labban, J. A. Bartelt, J. D. Douglas, W. R. Mateker, J. M. J. Fréchet, M. D. McGehee, P. M. Beaujuge, *J. Am. Chem. Soc.* **2013**, *135*, 4656.
[36] D. Baran, M. S. Vezie, N. Gasparini, F. Deledalle, J. Yao, B. C. Schroeder, T. Ameri, T. Kirchartz, I. McCulloch, J. Nelson, C. J. Brabec, unpublished.
[37] B. Carsten, F. He, H. J. Son, T. Xu, L. Yu, *Chem. Rev.* **2011**, *111*, 1493.
[38] H. Zhang, T. Stubhan, N. Li, M. Turbiez, G. J. Matt, T. Ameri, C. J. Brabec, *J. Chem. Mater. A* **2014**, *2*, 18917.
[39] V. Mihailetchi, J. Wildeman, P. Blom, *Phys. Rev. Lett.* **2005**, *94*, 126602.
[40] V. D. Mihailetchi, H. X. Xie, B. de Boer, L. J. A. Koster, P. W. M. Blom, *Adv. Funct. Mater.* **2006**, *16*, 699.
[41] T.-Y. Chu, J. Lu, S. Beaupré, Y. Zhang, J.-R. Pouliot, S. Wakim, J. Zhou, M. Leclerc, Z. Li, J. Ding, Y. Tao, *J. Am. Chem. Soc.* **2011**, *133*, 4250.
[42] N. Gasparini, S. Righi, F. Tinti, A. Savoini, A. Cominetti, R. Po, N. Camaioni, *ACS Appl. Mater. Interfaces* **2014**, *6*, 21416.
[43] G. J. R. O. A. Pivrikas, N. S. Sariciftci, *Progr. Photovoltaics Res. Appl.* **2007**, *15*, 677.
[44] A. Mozer, G. Dennler, N. Sariciftci, M. Westerling, A. Pivrikas, R. Österbacka, G. Juška, *Phys. Rev. B: Condens. Matter* **2005**, *72*, 035217.
[45] T. Kirchartz, U. Rau, M. Kurth, J. Mattheis, J. H. Werner, *Thin Solid Films* **2007**, *515*, 6238.
[46] T. Kirchartz, U. Rau, *J. Appl. Phys.* **2007**, *102*, 104510.
[47] R. A. Street, A. Krakaris, S. R. Cowan, *Adv. Funct. Mater.* **2012**, *22*, 4608.
[48] A. Gadisa, W. Mammo, L. M. Andersson, S. Admassie, F. Zhang, M. R. Andersson, O. Inganäs, *Adv. Funct. Mater.* **2007**, *17*, 3836.
[49] F. P. V. Koch, P. Smith, M. Heeney, *J. Am. Chem. Soc.* **2013**, *135*, 13695.